The Journal of Chemical Physics

RESEARCH ARTICLE | NOVEMBER 03 2022

Ab initio quantum scattering calculations for the CO–O_2 system and a new CO–O_2 potential energy surface: O_2 and air broadening of the R(0) line in CO

Adam Zadrożny ; Hubert Jóźwiak ; Ernesto Quintas-Sánchez ; Richard Dawes ; Piotr Wcisło

Check for updates

J. Chem. Phys. 157, 174310 (2022)
https://doi.org/10.1063/5.0115654
CHORUS

View Online
Export Citation

Articles You May Be Interested In

Ab initio quantum scattering calculations and a new potential energy surface for the HCl($X^1\Sigma^+$)–O_2(X 3 Σ g −) system: Collision-induced line shape parameters for O_2-perturbed R(0) 0–0 line in $H^{35}Cl$

J. Chem. Phys. (October 2023)

Fully quantum calculations of O_2–N_2 scattering using a new potential energy surface: Collisional perturbations of the oxygen 118 GHz fine structure line

J. Chem. Phys. (September 2021)

Ab initio investigation of the CO–N_2 quantum scattering: The collisional perturbation of the pure rotational R(0) line in CO

J. Chem. Phys. (February 2021)

09 March 2026 12:51:39

AIP Advances
Why Publish With Us?
21DAYS average time to 1st decision
OVER 4 MILLION views in the last year
INCLUSIVE scope
Learn More
AIP Publishing

AIP Publishing

The Journal of Chemical Physics ARTICLE scitation.org/journal/jcp

Ab initio quantum scattering calculations for the CO–O_2 system and a new CO–O_2 potential energy surface: O_2 and air broadening of the R(0) line in CO

Cite as: J. Chem. Phys. **157**, 174310 (2022); doi: 10.1063/5.0115654
Submitted: 27 July 2022 • Accepted: 28 September 2022 •
Published Online: 3 November 2022 • Publisher Error Corrected: 18 November 2022

View Online Export Citation CrossMark

Adam Zadrożny,[1,a] Hubert Jóźwiak,[1] Ernesto Quintas-Sánchez,[2] Richard Dawes,[2] and Piotr Wcisło[1,b]

AFFILIATIONS

[1] Institute of Physics, Faculty of Physics, Astronomy and Informatics, Nicolaus Copernicus University in Toruń, Grudziądzka 5, 87-100 Toruń, Poland

[2] Department of Chemistry, Missouri University of Science and Technology, Rolla, Missouri 65409-0010, USA

[a] **Author to whom correspondence should be addressed:** zadroznyadam@protonmail.com
[b] **Electronic mail:** piotr.wcislo@umk.pl

ABSTRACT

We present *ab initio* calculations of the collisional broadening of the R(0) pure rotational line in CO (at 115 GHz) perturbed by O_2. Our calculations are done in a fully quantum way by solving close-coupling quantum-scattering equations without any approximations. We also report a new, highly accurate CO–O_2 potential energy surface on which we did the quantum-scattering calculations. The calculated collisional broadening agrees with the available experimental data in a wide temperature range. The calculated collisional shift is negligible compared to the broadening, which is also consistent with the experimental data. We combine this result with our previous calculations for the same line in CO perturbed by N_2 [Jóźwiak *et al.*, J. Chem. Phys. **154**, 054314 (2021)]; the obtained air-perturbed broadening of the R(0) pure rotational line in CO and its temperature dependence perfectly agree with the HITRAN database. This result constitutes an important step toward developing a methodology for providing accurate *ab initio* reference data on spectroscopic collisional line-shape parameters for molecular systems relevant to the Earth's atmosphere and for populating spectroscopic line-by-line databases.

© 2022 Author(s). All article content, except where otherwise noted, is licensed under a Creative Commons Attribution (CC BY) license (http://creativecommons.org/licenses/by/4.0/). https://doi.org/10.1063/5.0115654

09 March 2026 12:51:39

I. INTRODUCTION

Carbon monoxide is one of the important trace gases used in the study of air quality and climate forcing.[1] While CO itself is not a greenhouse gas, it affects ozone and methane concentrations, thus contributing to climate change.[1–3] Remote sensing measurements of CO can also be used to monitor air quality and emissions from burning fossil fuels.[4–6] The oxygen molecule, O_2, is the second most abundant species in the Earth's atmosphere, constituting 21% of dry air. Thus, collisions with O_2 significantly affect the lineshapes of the less abundant absorbing compounds.

The first *ab initio* investigation of the interaction energy in the CO–O_2 system was performed by Grein,[7] who studied several geometries of the complex using the explicitly-correlated coupled-cluster method, CCSD(T)-F12, with single, double, and perturbative triple excitations. Tashakor *et al.*[8] calculated the potential energy surface (PES) of the CO–O_2 system with the CCSD(T) method with aug-cc-pVDZ and aug-cc-pVTZ basis sets extrapolated to the complete basis set limit (CBS). The authors considered 1260 geometries of the complex, keeping the angle between the intermolecular axis and the bond axis of the O_2 molecule fixed at 90° and 180°. Recently, some of the authors calculated a high-level *ab initio* four-dimensional (4D) PES for the CO–O_2 system,[9] which was used for the analysis of the infrared spectrum of the complex.

The experimental investigation of the collisional broadening of the pure rotational transitions in CO has a long history. In 1986,

© Author(s) 2022

measurements of CO, N_2, O_2 and air broadening of the R(0) line were published by Connor and Radford[10] and by Colmont and Monnanteuil.[11] In a later work, Nissen *et al.*[12] employed time and frequency domain techniques to study the broadening of the same line by CO, N_2, O_2 and noble gases. Other papers focused on the foreign-gas broadening of the lines R(1),[13] R(2),[14,15] and R(4).[16] A comparison of different line-shape models for the R(0) through R(4) pure rotational lines of ^{12}CO and ^{13}CO at room temperature can be found in the work of Puzzarini *et al.*[17] The only theoretical investigation of line-shape parameters in the O_2-perturbed pure rotational lines of CO was mentioned in Ref. 18. It was done for the R(4) line by Botanic, who, in unpublished work, used the semi-classical Robert–Bonamy formalism[19] and a simplified model of the interaction energy of the colliding pair based on the Lennard–Jones potential.

In this paper, we report a new highly accurate *ab initio* CO–O_2 PES (available in the supplementary material). We use it to calculate the line-shape of the pure rotational R(0) line in CO perturbed by O_2, using an exact close-coupling approach. We find that it is dominated by pressure broadening, with negligible collisional shift. Hence, we focus on the pressure broadening coefficient and its temperature dependence. The results are consistent with experimental data in the literature.[10–12] Finally, combining this result with a previous *ab initio* calculation of the broadening of the same line by N_2[20] allows us to determine the temperature dependence of the air-perturbed broadening of the R(0) line in CO, which agrees with the HITRAN database.[21]

This paper is organized as follows: In Sec. II, we introduce the potential energy surface and briefly describe the method of decomposing it into angular and radial terms. In Sec. III, we discuss the scattering calculations and analyze the generalized spectroscopic cross sections we obtained. In Sec. IV, we describe the calculation of the pressure broadening coefficient, and then, in Sec. V, we compare the calculated O_2-broadening with experimental data. We also compare the combined O_2 and N_2 broadening with the air-broadening coefficient from the HITRAN database. Finally, in Sec. VI, we summarize our results and put them in their broader context.

II. POTENTIAL ENERGY SURFACE

In the scattering calculations whose description follows, we use a 4D PES depending on the inter-molecular distance, R, the angles θ_1 and θ_2 between the inter-molecular axis and the axes of the molecules, and the relative dihedral angle between molecules (Fig. 1). Notice that for $\theta_1 = 0°$, the CO molecule aligns with the C atom pointing to the center-of-mass of the O_2 molecule.

For construction of the PES, both monomers were held rigid at their equilibrium bond distances (1.128 21 Å for CO, and 1.207 52 Å for O_2). The final high-level PES was computed using explicitly-correlated unrestricted coupled-cluster theory, UCCSD(T),[22] extrapolated to the complete basis limit, UCCSD(T)-F12/CBS. The basis extrapolation was performed using the VTZ-F12 and VQZ-F12 bases[23] and the l^{-3} formula.[24] In our experience with dimer complexes composed of a few light atoms, the binding energy and relative energies of vdW isomers are typically converged to within 1–2 cm^{-1} with this procedure, which does not employ

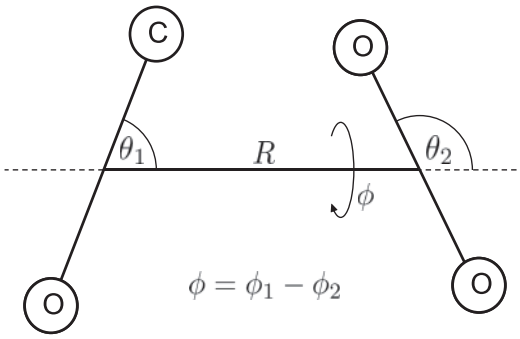

FIG. 1. Schematic representation of the CO–O_2 system in Jacobi coordinates.

counterpoise corrections or mid-bond functions. We have previously studied the effects of basis set convergence and core-correlation on the isomers of this system and also studied the rovibrational levels in comparison with experiments.[9,25] Those previous studies support the accuracy of our new PES. All *ab initio* calculations were performed using the Molpro electronic structure code package.[26] Stable convergence to the restricted open-shell Hartree–Fock (roHF) reference was achieved by first using Molpro's complete active space self-consistent field (CASSCF) (multi) algorithm with the occupation of the desired configuration specified, followed by a single iteration of the roHF SCF algorithm to prepare the orbitals for the UCCSD(T)-F12b procedure. As mentioned below, to avoid placing expensive high-level data in energetically inaccessible regions, a lower-level guide surface was first constructed. This was done using data at the UCCSD(T)-F12a/VDZ-F12 level of theory. The guide surface is only used to aid in the efficient construction of the high-level PES, on which all evaluations used to study the dynamics were performed. Exploiting the system's symmetry, energies were only computed in the reduced angular range: $0° < \theta_1 < 180°$, $0° < \theta_2 < 90°$, and $0° < \phi < 180°$.

As we have done in the past for other vdW linear dimers,[27–34] an analytical representation of the PES was constructed using an automated interpolating moving least squares (IMLS) methodology, freely available as a software package under the name AUTOSURF.[35] As usual,[36,37] a local fit was expanded around each data point, and the final potential was obtained as the normalized weighted sum of the local fits. The fitting basis and other aspects of the procedure were the same as for other previous systems and have been described in detail elsewhere.[35,37,38] The shortest intermonomer center-of-mass distance considered is $R = 2.3$ Å, and the *ab initio* data coverage in the fitted PES extends to $R = 20.0$ Å, while the zero of energy is set at infinite center-of-mass separation between the monomers. To represent the long range (out to arbitrary distances), the PES switches smoothly to an analytic expression representing electrostatic and dispersion interactions between the fragments (both truncated after seventh order). The parameters were obtained by fitting them to the *ab initio* data with $R > 8.0$ Å. Induction was neglected as the fitted parameters were small and did not improve the fit. For the high-level PES, 2936 symmetry-unique points were required to achieve an estimated root-mean-squared fitting error of 0.04 cm^{-1} for energies below the asymptote. To guide the placement of high-level data, a lower-level guide surface was constructed using

09 March 2026 12:51:39

© Author(s) 2022

1434 symmetry-unique points, distributed using a Sobol sequence[39] biased to sample the short-range region more densely.

Figure 2 shows a 2D representation of the PES (denoted R-optimized) as a function of the angles θ_1 and θ_2 for planar ($\phi = 0°$) and crossed ($\phi = 90°$) configurations. The plot describes the complete ranges of θ_1 and θ_2, relaxing the intermonomer distance coordinate R for each pair of angles. As can be seen in the figure, three stable isomers exist. The global minimum (GM) has a well depth of 120.7 cm^{-1} and corresponds to a planar ($\phi = 0°$) slipped parallel configuration with the O-atom of CO oriented toward the O_2 molecule. For the GM, θ_1 and θ_2 are close to 100°. A second planar local minimum exists (LM1), with a well depth of 112.1 cm^{-1} and also a slipped parallel structure, but with the C-atom of CO oriented toward the O_2 molecule. In LM1, the twist is more pronounced, with both angles found near 60°. Finally, a third minimum (LM2) corresponds to a non-planar nearly cross-shaped structure, with the CO fragment tipped very slightly ($\theta_1 = 88.6°$) so that the C-atom is closer to the O_2 fragment. The geometric parameters of the three minima in the PES are given in Table I.

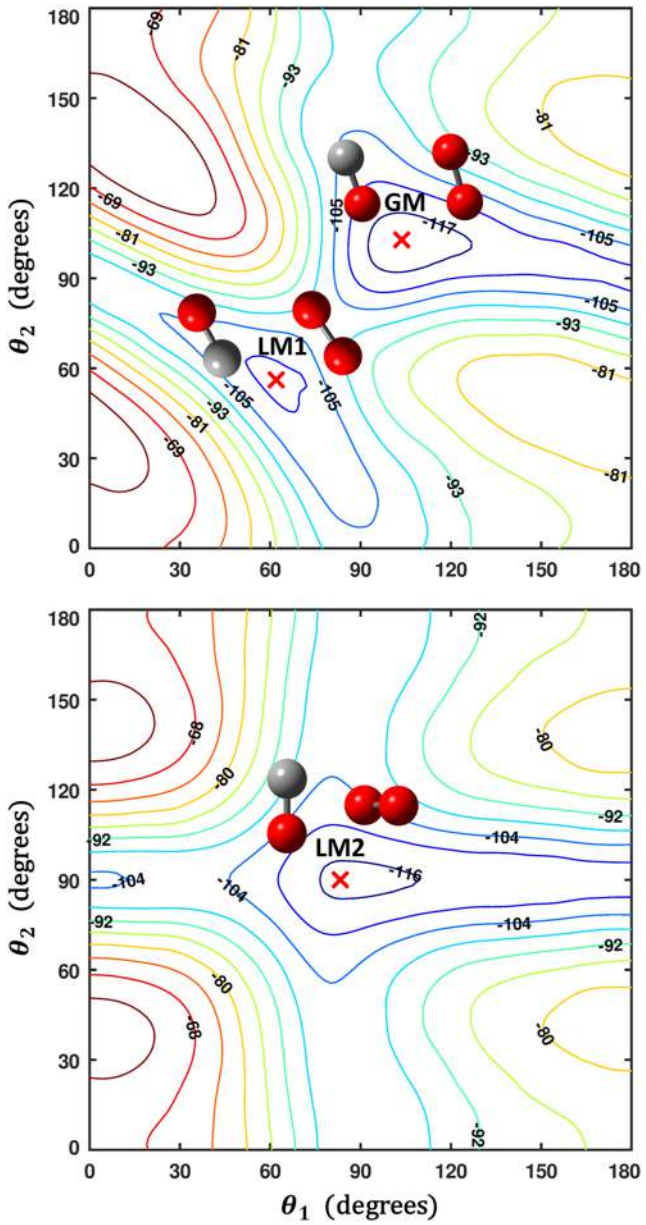

FIG. 2. R-optimized contour plots of the PES as a function of the angles θ_1 and θ_2, with the torsion fixed at $\phi = 0°$ (upper panel) and $\phi = 90°$ (lower panel). For each pair of angles, the energy (given in cm^{-1}) is optimized with respect to the center-of-mass distance R.

TABLE I. Geometric parameters and potential energy for equilibrium structures as shown in Fig. 2. Units are Å, degrees, and cm^{-1}.

	GM	LM1	LM2
R	3.459	3.820	3.450
θ_1	104.8	61.7	88.6
θ_2	101.1	56.3	90.0
ϕ	0.0	0.0	90.0
V	−120.7	−112.1	−117.3

Figure 3 shows the potential as a function of R upon approach for different fixed angular configurations, including those corresponding to the three minima of the PES. The variation in those cuts gives some indication of the anisotropy of the interactions. The strength and anisotropy of the PES describing the interaction between collision partners govern the scattering dynamics and, hence, the derived line shape parameters.

To use the PES in scattering calculations, one needs to separate the radial and angular dependence, which can be achieved

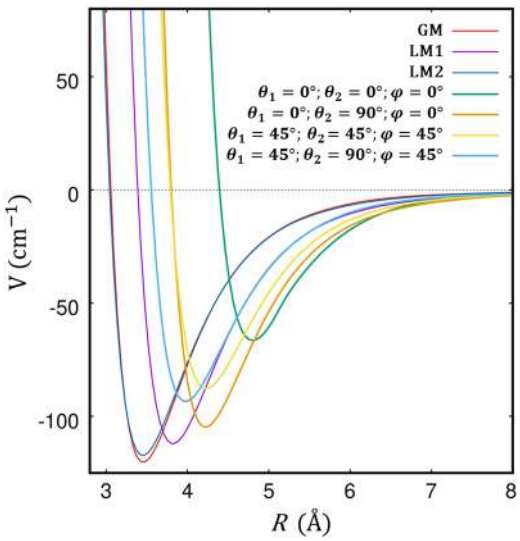

FIG. 3. Radial cuts through the PES are shown for a series of fixed angular poses, including those corresponding to the stationary points highlighted in Fig. 2.

09 March 2026 12:51:39

© Author(s) 2022

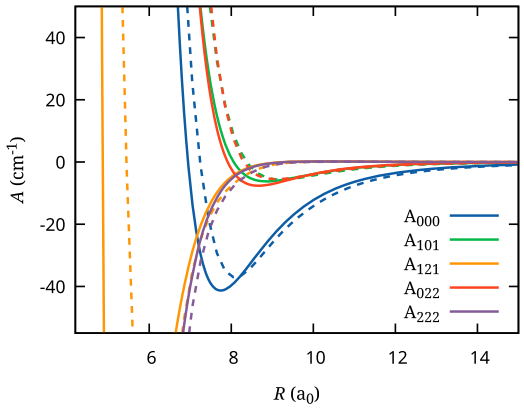

FIG. 4. Comparison between the PES radial terms for CO–O_2 and CO–N_2 systems (solid and dashed lines, respectively). As can be observed, they generally have a similar shape but with the CO–O_2 PES being somewhat deeper and the repulsive wall at a closer distance. Note that the radial terms are shown divided by a factor of $8\pi^2/(2l+1)$ compared to Eq. (3).

by expanding the potential over bispherical harmonics, which are given by[40]

$$I_{l_1 l_2 l}(\theta_1,\theta_2,\phi) = \sqrt{\frac{2l+1}{4\pi}}\sum_m (l_1\, m\, l_2\, -m\,|\,l_1\, l_2\, l\, 0) \times Y_{l_1 m}(\theta_1,\phi_1) Y_{l_2 -m}(\theta_2,\phi_2), \quad (1)$$

where $Y_{l_i m_i}(\theta_i,\phi_i)$ denotes the usual spherical harmonic for each of the molecules, and $(l_1 m\, l_2 - m|l_1 l_2 l\, 0)$ is the Clebsch–Gordan coefficient. The quantum numbers l_1, l_2, and l can take non-negative integer values, while l_2 must also be even, given the symmetry of the O_2 molecule. They must also satisfy the triangle condition and must sum to an even integer.

Given the bispherical harmonics, the potential can be written as

$$V(R,\theta_1,\theta_2,\phi) = \sum_{l_1,l_2,l} A_{l_1 l_2 l}(R) I_{l_1 l_2 l}(\theta_1,\theta_2,\phi), \quad (2)$$

where the radial terms, $A_{l_1 l_2 l}(R)$, can be obtained by integration,

$$A_{l_1 l_2 l}(R) = \frac{8\pi^2}{2l+1}\int_0^{2\pi} d\phi \int_0^{\pi} \sin\theta_1 d\theta_1 \int_0^{\pi} \sin\theta_2 d\theta_2 \times V(R,\theta_1,\theta_2,\phi) I_{l_1 l_2 l}(\theta_1,\theta_2,\phi). \quad (3)$$

The factor $8\pi^2/(2l+1)$ comes up because of the normalization of the bispherical harmonics; see Ref. 41 for further discussion. The radial terms were calculated for all possible values of (l_1, l_2, l) up to $(10, 8, 18)$ on a uniform grid of 916 values of R between 4.25 a_0 and 50 a_0. The integration over θ_1 and θ_2 was performed using the 22-point Gauss–Legendre quadrature and integration over ϕ using the 21-point Simpson rule. Figure 4 shows a comparison of the CO–O_2 radial terms with terms obtained in this work with the corresponding terms for CO–N_2 calculated in Ref. 20.

III. SCATTERING CALCULATIONS

The theory underlying quantum-mechanical scattering calculations for two rigid diatomic molecules is well developed.[40,42,43] The radial terms described in Sec. II [Eq. (3)] are used to solve the close-coupling equations[40] for the radial wavefunction, $F^J_{j_1 j_2 j_{12} L}(R)$,

$$\left(\frac{d^2}{dR^2} - \frac{L(L+1)}{R^2} + k^2\right) F^J_{j_1 j_2 j_{12} L}(R) = 2\mu \sum_{j_1' j_2' j_{12}' L'} V^{J;\, j_1' j_2' j_{12}' L'}_{j_1 j_2 j_{12} L}(R) \times F^J_{j_1' j_2' j_{12}' L'}(R), \quad (4)$$

where L denotes the angular momentum of the relative motion of the molecules and μ is the reduced mass of the system. The angular momenta are coupled such that $j_{12} = j_1 + j_2$ and $J = j_{12} + L$. The squared wave vector, $k^2 = 2\,\mu(E - E_{j_1} - E_{j_2})$, describes the kinetic collisional energy. E is the kinetic energy, and E_{j_1} and E_{j_2} are the rotational energies of the CO and O_2 molecules, respectively. $V^{J;\, j_1' j_2' j_{12}' L'}_{j_1 j_2 j_{12}}$ is the coupling matrix element obtained by integrating the potential over all coordinates except R, which is conveniently achieved[40] using the radial term expansion [Eq. (3)]. The coupling is independent of projection M and occurs only between states of the same J and the same parity,[40] defined as $(-1)^{J+j_1+j_2+L}$. By matching the asymptotic behaviour of the radial wavefunction to the boundary condition, one can obtain the scattering matrix elements, which are then used to calculate the generalized spectroscopic cross sections, σ_0^q, with q signifying the tensor rank of radiation–matter interaction.

The generalized spectroscopic cross section in the case of diatom–diatom scattering can be written as follows:[44,45]

$$\sigma_0^q(j_i, j_f, j_2, E_{\rm kin}) = \frac{\pi}{k^2}\sum_{j_2'}\sum_{L,L',\bar{L},\bar{L}'}\sum_{J,j_{12},j_{12}',\bar{j}_{12},\bar{j}_{12}'} i^{L-L'-\bar{L}+\bar{L}'}(-1)^{j_2-j_2'+j_i-j_i'+L-L'-\bar{L}+\bar{L}'} \times [J][\bar{J}]\sqrt{[L][L'][\bar{L}][\bar{L}'][j_{12}][j_{12}'][\bar{j}_{12}][\bar{j}_{12}']}\begin{pmatrix} L & \bar{L} & 0\\ 0 & 0 & 0\end{pmatrix}\begin{pmatrix} L' & \bar{L}' & 0\\ 0 & 0 & 0\end{pmatrix}\begin{Bmatrix} q & j_{12}' & \bar{j}_{12}'\\ j_2' & j_f' & j_i'\end{Bmatrix}\begin{Bmatrix} q & \bar{j}_{12} & j_{12}\\ j_2 & j_i & j_f\end{Bmatrix} \times \begin{bmatrix} j_{12} & j_{12}' & \bar{L} & \bar{L}'\\ \bar{j}_{12} & L & \bar{j}_{12}' & L'\\ q & \bar{J} & J & 0\end{bmatrix}\left(\delta_{j_i j_f j_2 j_{12}\bar{j}_{12} L\bar{L} j_i' j_f' j_2' j_{12}' \bar{j}_{12}' L'\bar{L}'} - \langle j_i j_2 j_{12} L|S^J|j_i' j_2' j_{12}' L'\rangle\langle j_f j_2 \bar{j}_{12}\bar{L}|S^J|j_f' j_2' \bar{j}_{12}'\bar{L}'\rangle\right), \quad (5)$$

09 March 2026 12:51:39

© Author(s) 2022

where $[x] = 2x + 1$ and $\delta_{a\ldots z,a'\ldots z'} = \delta_{aa'}\ldots\delta_{zz'}$. The quantities $(\cdots)$, $\{\cdots\}$ and $[\cdots]$ are Wigner 3-j, 6-j and 12-j symbols, respectively.[46] The active molecule is the one undergoing a transition; its initial and final rotational levels are denoted by j_i and j_f. For the R(0) line considered in this paper, $j_i = 0$ and $j_f = 1$. The perturber's rotational levels are denoted as j_2. The tensor order of radiation–matter interaction is given by q. In the case of the electric dipole transition, considered in this work, $q = 1$.

We use a newly developed Fortran quantum-scattering code, BIGOS,[47] to carry out the calculations. BIGOS propagates the solutions using a renormalized Numerov Algorithm.[48] The propagation was carried out on an evenly-spaced grid of 916 values between 4.5 a_0 and 50.0 a_0 with 15 steps per half de Broglie wavelength for various energies up to 200 cm^{-1}.

The criterion for determining the maximum value of J needed for convergence, J_{max}, was that the largest partial elastic and inelastic state-to-state cross sections for four consecutive values of J contributed less than 10^{-3} Å^2. The final values of J_{max} used in the scattering calculations started from $J_{max} = 100$ for $E_{kin} < 30$ cm^{-1}, reaching $J_{max} = 150$ at about 70 cm^{-1}, and $J_{max} = 210$ at 200 cm^{-1}.

The energy basis was fixed and consisted of 36 energy levels, as shown in Table II. The same basis was used for all the calculations. The choice is based on our tests, which showed that convergence of the cross sections required many closed channels for energies below 25 cm^{-1}, while the cross sections for energies above 100 cm^{-1} the stated basis was enough to reach convergence of the cross sections below 1% with respect to a fully converged basis. The amount of memory and time required for the calculations grows considerably with basis size. Thus, in order to be able to perform the calculations for energies necessary to probe the regime where the cross sections follow a simple power law, we use an effectively truncated basis for energies above 130 cm^{-1}, trading computation time for accuracy.

The energy basis described above allows for the calculation of scattering cross sections for the first four rotational states of the perturbing molecule, O_2, that is, $j_2 = 1, 3, 5, 7$. We found the imaginary part of σ_0^1 to be two orders of magnitude smaller than the real part. Considering this and the fact that no significant pressure shift for the O_2-perturbed CO lines has been detected in any experiments,[10–12] we will present only the results for the broadening cross sections ($\mathrm{Re}\,\sigma_0^1$). Figure 5 shows the dependence of $\mathrm{Re}\,\sigma_0^1$ on collisional kinetic energy. It can be seen that pressure broadening cross sections become approximately independent of the perturber's rotational state at high energies. Similar behavior has been observed for other systems, such as N_2–H_2,[50] N_2–N_2,[51] CO–N_2,[20] and O_2–N_2.[32] We use this observation to extrapolate $\mathrm{Re}\,\sigma_0^1$ for higher rotational levels, assuming $\mathrm{Re}\,\sigma_0^1(E_{kin}; j_2) = \mathrm{Re}\,\sigma_0^1(E_{kin}; 7)$.

Resonant structures can be seen for the pressure broadening cross section at $j_2 = 1$ at kinetic energies below about 70 cm^{-1}. No significant resonances were observed for other j_2 values. The resonances die out before reaching the regime of most probable energies (see Fig. 6), which justifies neglecting their impact on the pressure broadening [Eqs. (7) and (10)]; see also the discussion in Chap. VI of Ref. 20.

In order to extrapolate $\mathrm{Re}\,\sigma_0^1$ to higher kinetic energies, we use another observation. For each rotational energy level, starting from

TABLE II. Energy levels (in cm^{-1}) used in the calculations of generalized spectroscopic cross sections. Each entry in the table corresponds to the sum $E_{j_1} + E_{j_2}$ of CO and O_2 rotational energy levels. Due to the symmetry of the O_2 molecule, only the levels with an odd rotational quantum number are possible. The energy levels for the CO molecule were taken from the HITRAN database,[21] while the O_2 levels were calculated from the effective Hamiltonian.[49]

	j_2			
j_1	1	3	5	7
0	2.88	17.26	43.14	80.51
1	6.72	21.10	46.98	84.36
2	14.41	28.79	54.67	92.05
3	25.95	40.32	66.21	103.58
4	41.32	55.70	81.58	118.96
5	60.55	74.93	100.81	138.18
6	83.61	98.00	123.87	161.25
7	110.52	124.90	150.78	188.16
8	141.27	155.66	181.53	218.90

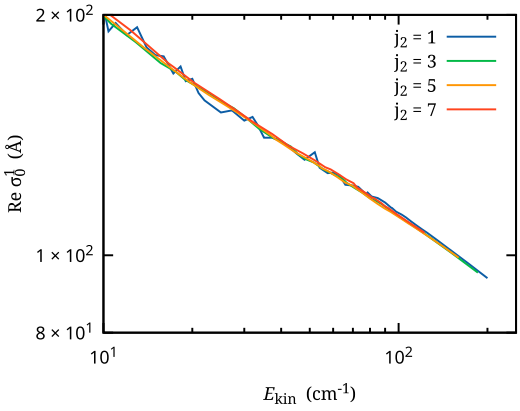

FIG. 5. Pressure broadening cross sections, $\mathrm{Re}\,\sigma_0^1$, for the first four rotational levels of the perturber as a function of relative kinetic energy.

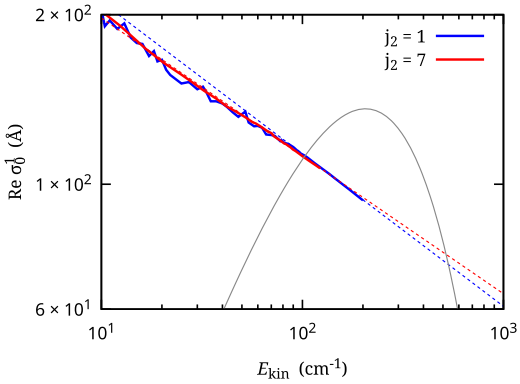

FIG. 6. *Ab initio* pressure broadening cross sections together with power-law fits. Maxwell–Boltzmann distribution (in arbitrary units) at 296 K added for reference.

09 March 2026 12:51:39

© Author(s) 2022

TABLE III. Coefficients of the power-law fit and corresponding cutoff energies E_{cutoff} for different rotational levels of the perturber. The values in parentheses correspond to standard deviations.

j_2	A (cm^{-1})	b	E_{cutoff} (cm^{-1})
1	113.16(5)	0.270(1)	90
3	111.72(6)	0.253(2)	65
5	111.57(4)	0.241(1)	45
7	112.28(9)	0.245(2)	45

a certain cutoff energy, the pressure broadening cross section energy dependence is linear on a log-log plot, meaning it follows a power law relationship. We perform a numerical fit,

$$\sigma_0^1(E_{\text{kin}}) = A\left(\frac{E_0}{E_{\text{kin}}}\right)^b, \tag{6}$$

taking the reference energy $E_0 = 100$ cm^{-1}. The fit coefficients, A and b, along with corresponding cutoff energies are presented in Table III. Figure 6 presents the power law fits for chosen rotational levels.

Based on the above observations, we apply the following procedure to obtain $\text{Re}\,\sigma_0^1$ values for arbitrary j_2 and E_{kin} needed for line-shape integrals (see Sec. IV): below cutoff energies, we take the *ab initio* values, and above the cutoffs the extrapolated values are used, substituting $j_2 = 7$ for rotational levels with $j_2 > 7$.

IV. LINE-SHAPE PARAMETERS

The broadening and shift line-shape parameters, γ and δ, are related to their pressure-dependent counterparts by $\Gamma = \gamma p$ and $\Delta = \delta p$. The speed-averaged pressure broadening coefficient, γ_0, at a given temperature, T, can be obtained directly from the generalized spectroscopic cross sections,[52]

$$\gamma_0 = \frac{1}{2\pi c}\frac{\bar{v}_r}{k_B T}\sum_{j_2} p_{j_2}\,\text{Re}\int_0^\infty dx\, e^{-x}\sigma_0^1(j_i, j_f, j_2, x), \tag{7}$$

where j_i and j_f denote the initial and final states of the active molecule. For the R(0) line considered in this paper, $j_i = 0$ and $j_f = 1$. $x = E_{\text{kin}}/k_B T$ and $\bar{v}_r = \sqrt{8k_B T/\pi\mu}$ denotes the mean relative speed of the molecules with reduced mass μ. The factor $1/(2\pi c)$, where c is the speed of light, is responsible for the conversion from units of angular frequency to wave numbers. The weights p_{j_2} correspond to the populations of the rotational levels j_2 of the perturbing molecule at a given temperature and can be expressed as

$$p_{j_2}(T) = \frac{1}{Z(T)}(2j_2 + 1)\exp\left(-\frac{E_{j_2}}{k_B T}\right), \tag{8}$$

where E_{j_2} denotes the energy of the j_2th rotational level and $Z(T)$ is the partition function,

$$Z(T) = \sum_{j_2}(2j_2 + 1)\exp\left(-\frac{E_{j_2}}{k_B T}\right). \tag{9}$$

In all the calculations, we carried out the summations up to $j_2 = 39$, covering more than 99.9% of the population of the perturber's rotational states at room temperature.

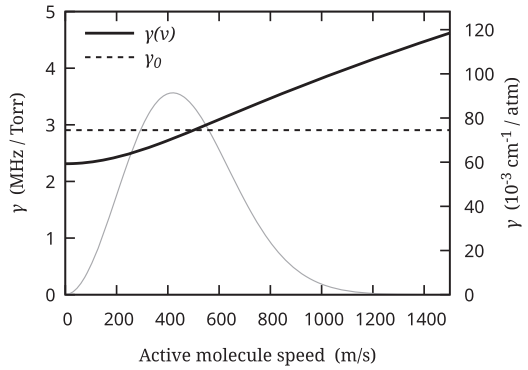

FIG. 7. *Ab initio* speed dependence of pressure broadening $\gamma(v)$ (solid black line) and speed-averaged coefficient, γ_0 (dashed line) at 296 K. The gray curve represents the Maxwell–Boltzmann distribution of speeds of the active molecule (in arbitrary units).

To obtain the dependence of the pressure broadening coefficient on the active molecule speed, v, one can use the following formula:[52]

$$\gamma(v) = \frac{1}{2\pi c}\frac{1}{k_B T}\frac{2}{\sqrt{\pi}v_p v}\sum_{j_2} p_{j_2}\,\text{Re}\int_0^\infty dv_r\, v_r^2 \times e^{-\frac{v^2+v_r^2}{v_p^2}}\sinh\left(\frac{2vv_r}{v_p^2}\right)\sigma_0^1(j_i, j_f, j_2, v_r), \tag{10}$$

where v_r denotes the relative speed of the monomers and $v_p = \sqrt{2k_B T/m_p}$ is the most probable speed of the perturber and the generalized spectroscopic cross section $\sigma_0^1(j_i, j_f, j_2, v_r)$ is defined in Eq. (5).

Figure 7 shows the comparison of γ_0 and $\gamma(v)$ at 296 K calculated using Eqs. (7) and (10), along with the corresponding Maxwell–Boltzmann distribution.

The speed dependence of a pressure broadening coefficient manifests itself in the effective width of the spectral line being narrower than predicted by γ_0. For each velocity, the line will have a Lorentz profile; therefore, to find the effective width one needs to average over the Maxwell distribution $f_m(\vec{v})$, obtaining a weighted sum of Lorentz profiles (WSLP),

$$I_{\text{WSLP}}(\nu - \nu_0') = \frac{1}{\pi}\int_0^\infty d^3\vec{v} f_m(\vec{v})\frac{\Gamma(v)}{\Gamma^2(v) + (\nu - \nu_0')^2}, \tag{11}$$

where ν_0' denotes line position, including the speed-dependent pressure shift, which we disregard, taking $\nu_0' = \nu_0$. Fitting a single Lorentz profile to the resultant WSLP yields the effective width, which can be compared with experimental data.[10–12]

V. COMPARISON WITH EXPERIMENTAL DATA

We calculate pressure broadening coefficients for a range of temperatures between 200 and 320 K and fit them to an empirical power law,

$$\gamma(T) = \gamma(T_0)\left(\frac{T_0}{T}\right)^n, \tag{12}$$

with T_0 being a reference temperature, in our case 296 K.

09 March 2026 12:51:39

© Author(s) 2022

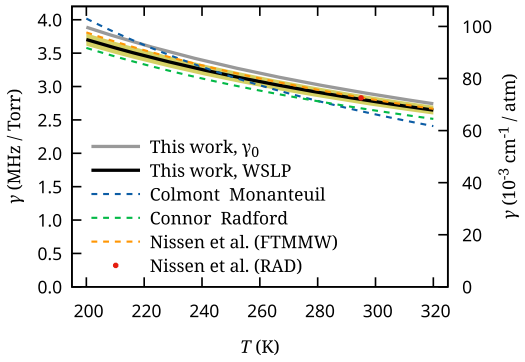

FIG. 8. Comparison between *ab initio* and experimental temperature dependence of pressure broadening. References to experimental papers are given in Table IV.

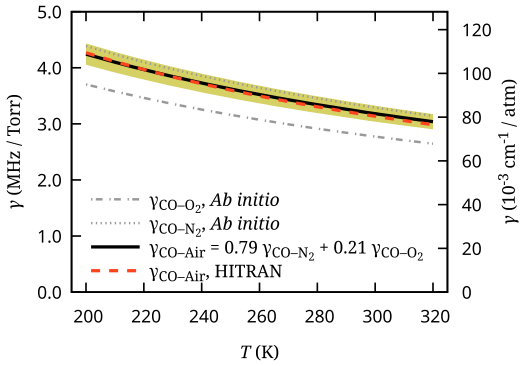

FIG. 9. Comparison of *ab initio* air-induced pressure broadening coefficient (γ_{CO-Air}) with HITRAN2020 data.[21,53,54] The γ_{CO-O_2} (from this work) and γ_{CO-N_2} (from Ref. 20) *ab initio* values from which γ_{CO-Air} was calculated were added for reference. The shaded region corresponds to an estimated uncertainty of 4.5% of our result, based on the uncertainties of γ_{CO-O_2} (2.5%) and γ_{CO-N_2} (5%).

Figure 8 shows a comparison between the temperature dependence of *ab initio* pressure broadening and available experimental data. The fit parameters are shown in Table IV. Our results agree with the experimental data, especially after including the speed dependence through the WSLP model. The shaded region corresponds to an estimated total uncertainty of 2.5% of the final result, which includes the contributions from a number of different sources described below.

The dominant uncertainty in our calculations comes from the choice of computational basis size. Increasing its size from 36 (with $j_{1max} = 8$ and $j_{2max} = 7$) to 50 levels ($j_{1max} = 9$ and $j_{2max} = 9$) could change the broadening cross sections by up to 1.7%. Another factor influencing the results comes from the extrapolation of the kinetic energy dependence of $\mathrm{Re}\,\sigma_0^1$. In the final calculations, we use the cutoffs stated in Table III, taking *ab initio* points below the cutoffs and using the fit function above them. To estimate the effect of their choice on the final results, we varied them in the range of ± 20 cm^{-1}. The results obtained that way differed by up to 0.6%. The final contribution to the uncertainty of the calculations comes from the choice of parameters of the propagator used to solve the close coupling equations (R_{min}, R_{max}, and step size). The starting point of the propagation, R_{min}, should be set deep in the classically forbidden region, where interaction is strongly repulsive, while at the ending point, R_{max}, the radial terms must vanish, allowing for application of the boundary conditions. We estimate the influence of R_{min} and R_{max} at 0.1% each. To choose the step size (expressed equivalently as a number of steps per half de Broglie wavelength), we ran sample calculations with the number of steps varying from 15 to 50. We found no significant difference in the results, so in the interest of speed, we chose the number of steps to be 15 in the final calculations. Taking all the sources of uncertainty described above (basis size, extrapolation cutoffs, and propagation parameters), we estimate the total uncertainty of the pressure broadening cross sections at 2.5%.

TABLE IV. Comparison of available experimental power law coefficients [Eq. (12)] and *ab initio* values. The quantities in parentheses represent the standard deviation of the experimental data and the estimated uncertainty of our theoretical results.

Experiment	T_0 (K)	γ (MHz/Torr)	n
Nissen *et al.* (RAD)[12]	296	2.83(2)	...
Nissen *et al.* (FTMMW)[12]	300	2.80(1)	0.76(2)
Colmont and Monanteuil[11]	293	2.65(10)	1.09(13)
Connor and Radford[10]	300	2.64(11)	0.75(10)
This work, γ_0	296	2.91(7)	0.744(2)
This work, WSLP	296	2.80(7)	0.715(2)

Combining our results for the O_2 broadening coefficient of the R(0) line of CO with analogous calculations for N_2-induced broadening published in Ref. 20, we are able to calculate the air-broadening coefficient, γ_{CO-Air} (see Fig. 9), using the following relation:

$$\gamma_{CO-Air} = 0.79\gamma_{CO-N_2} + 0.21\gamma_{CO-O_2}, \quad (13)$$

where γ_{CO-N_2} and γ_{CO-O_2} are WSLP broadening coefficients. The values of γ_{CO-Air} obtained this way are in excellent agreement with air-broadened half-widths from the HITRAN2020 database[21] based on the work of Hashemi *et al.*,[53] which found the vibrational band dependence of the half-widths to be negligible (below 1% on average, see Fig. 12 in Ref. 53). The cited values are a result of fitting the measured air-broadening data for several bands simultaneously, including measurements for 1–0, 2–0 and 3–0 bands from Refs. 55–57 and expanding the results for all the air-broadened transitions of CO.

VI. CONCLUSIONS

In this paper, we presented the first theoretical calculation of the O_2-induced pressure broadening of the R(0) spectral line in the CO molecule. We also reported a new highly accurate CO–O_2 PES on which we did the quantum-scattering calculations (the PES is provided as a supplementary material). We calculated the generalized spectroscopic cross sections for the first four rotational levels of the perturber for energies up to 200 cm^{-1} from the close-coupling equations without the use of any further dynamical approximations. This allowed us to obtain the temperature dependence of the pressure broadening coefficient, which we found to be in good agreement with experimental data. Furthermore, by combining our results with the results of a previous study concerning CO–N_2, we

09 March 2026 12:51:39

© Author(s) 2022

also calculated the temperature dependence of the air-broadening coefficient, obtaining a very good agreement with HITRAN data. This work is part of an effort concerning theoretical investigations of collisional effects on the structure of rotational lines involving molecules of atmospheric importance.

Apart from collisional broadening and its speed dependence, *ab initio* calculations can provide collisional shift (and its speed dependence), as well as the complex frequency of optical velocity changing collisions,[52] which deteriorate the shape of molecular resonances. These quantities are often not large enough to be detected in the experiment, and thus calculations from first principles might serve as reference data for future measurements. We note here that the first two *ab initio* databases provided in Refs. 58 and 59 for H_2–He and HD–He involve line shape parameters for thousands of lines, for which measurements of collisional parameters have never been performed. The work presented here constitutes the first step toward a similar database for the O_2-perturbed lines in the CO molecule.

SUPPLEMENTARY MATERIAL

The new 4D CO–O_2 potential energy surface on which the calculations were performed is available as a supplementary material.

ACKNOWLEDGMENTS

H.J. and P.W. were supported by the National Science Centre in Poland through Project No. 2018/31/B/ST2/00720. A.Z. was supported by the National Science Centre in Poland through Project No. 2020/39/B/ST2/00719. R.D. and E.Q.-S. were supported by the U.S. Department of Energy (Award No. DE-SC0019740). This research is a part of the program of the National Laboratory FAMO in Toruń, Poland. Calculations were partially carried out using resources provided by the Wroclaw Center for Networking and Supercomputing (http://wcss.pl), Grant No. 546. This research was supported, in part, by PLGrid Infrastructure.

AUTHOR DECLARATIONS

Conflict of Interest

The authors have no conflicts to disclose.

Author Contributions

Adam Zadrożny: Formal analysis (equal); Investigation (lead); Software (equal); Visualization (equal); Writing – original draft (lead). **Hubert Jóźwiak**: Methodology (equal); Software (lead); Validation (equal); Writing – original draft (supporting); Writing – review & editing (equal). **Ernesto Quintas-Sánchez**: Methodology (equal); Software (equal); Visualization (equal); Writing – original draft (supporting); Writing – review & editing (supporting). **Richard Dawes**: Methodology (equal); Software (equal); Visualization (equal); Writing – original draft (supporting); Writing – review & editing (supporting). **Piotr Wcisło**: Conceptualization (equal); Funding acquisition (equal); Methodology (equal); Project administration (equal); Supervision (equal); Validation (equal); Writing – review & editing (lead).

DATA AVAILABILITY

The data that support the findings of this study are available within the article and its supplementary material.

REFERENCES

[1] M. George, C. Clerbaux, D. Hurtmans, S. Turquety, P.-F. Coheur, M. Pommier, J. Hadji-Lazaro, D. P. Edwards, H. Worden, M. Luo *et al.*, "Carbon monoxide distributions from the IASI/METOP mission: Evaluation with other space-borne remote sensors," Atmos. Chem. Phys. **9**, 8317–8330 (2009).
[2] J. C. Carole, W. W. White, and N. Beale, *Global Climate Change Linkages: Acid Rain, Air Quality, and Stratospheric Ozone* (Springer Science & Business Media, 1989).
[3] J. S. Daniel and S. Solomon, "On the climate forcing of carbon monoxide," J. Geophys. Res.: Atmos. **103**, 13249–13260, https://doi.org/10.1029/98jd00822 (1998).
[4] C. Shan, W. Wang, C. Liu, Y. Sun, Q. Hu, X. Xu, Y. Tian, H. Zhang, I. Morino, D. W. T. Griffith, and V. A. Velazco, "Regional CO emission estimated from ground-based remote sensing at Hefei site, China," Atmos. Res. **222**, 25–35 (2019).
[5] R. D. Stephens and S. H. Cadle, "Remote sensing measurements of carbon monoxide emissions from on-road vehicles," J. Air Waste Manage. Assoc. **41**, 39–46 (1991).
[6] W. McMillan, R. Pierce, L. Sparling, G. Osterman, K. McCann, M. Fischer, B. Rappenglueck, R. Newsom, D. Turner, C. Kittaka *et al.*, "An observational and modeling strategy to investigate the impact of remote sources on local air quality: A Houston, Texas, case study from the Second Texas Air Quality Study (TexAQS II)," J. Geophys. Res.: Atmos. **115**, D01301, https://doi.org/10.1029/2009jd011973 (2010).
[7] F. Grein, "High-level ab initio studies of the complex formed between CO and O_2," Chem. Phys. **488–489**, 11–16 (2017).
[8] S. Tashakor, M. R. Noorbala, and M. Namazian, "Ab initio study of the intermolecular potential energy surface for the ground electronic state of the O_2–CO system and prediction of second virial coefficients," Theor. Chem. Acc. **136**, 118 (2017).
[9] A. J. Barclay, A. R. W. McKellar, N. Moazzen-Ahmadi, R. Dawes, X.-G. Wang, and T. Carrington, "Infrared spectrum and intermolecular potential energy surface of the CO–O_2 dimer," Phys. Chem. Chem. Phys. **20**, 14431–14440 (2018).
[10] B. J. Connor and H. E. Radford, "Pressure broadening of the CO J = 1-0 rotational transition by N_2, O_2, and air," J. Mol. Spectrosc. **119**, 229–231 (1986).
[11] J. M. Colmont and N. Monnanteuil, "Self, nitrogen and oxygen broadening of the 115-GHz line of carbon monoxide," J. Quant. Spectrosc. Radiat. Transfer **35**, 81–85 (1986).
[12] N. Nissen, J. Doose, A. Guarnieri, H. Mäder, V. N. Markov, G. Y. Golubyatnikov, I. I. Leonov, V. N. Shanin, and A. F. Krupnov, "Foreign gas broadening studies of the $J' \leftarrow J = 1 \leftarrow 0$ rotational line of CO by frequency and time domain techniques," Z. Naturforsch. A **54**, 218–224 (1999).
[13] N. Semmoud-Monnanteuil and J. M. Colmont, "Pressure broadening of millimeter lines of carbon monoxide," J. Mol. Spectrosc. **126**, 210–219 (1987).
[14] D. Priem, F. Rohart, J.-M. Colmont, G. Wlodarczak, and J.-P. Bouanich, "Lineshape study of the J = 3 ← 2 rotational transition of CO perturbed by N_2 and O_2," J. Mol. Struct. **517–518**, 435–454 (2000).
[15] J.-P. Bouanich and C. Brodbeck, "Mesure des largeurs et des deplacements des raies de la bande 0 → 2 de CO autoperturbe et perturbe par N_2, O_2, H_2, HCl, NO et CO_2," J. Quant. Spectrosc. Radiat. Transfer **13**, 1–7 (1973).
[16] V. N. Markov, G. Y. Golubiatnikov, V. A. Savin, D. A. Sergeev, A. Guarnieri, and H. Mäder, "Line broadening and shifting studies of the J = 5 ← 4 transition of carbon monoxide perturbed by CO, N_2, and O_2," J. Mol. Spectrosc. **212**, 1–5 (2002).
[17] C. Puzzarini, L. Dore, and G. Cazzoli, "A comparison of lineshape models in the analysis of modulated and natural rotational line profiles: Application to the pressure broadening of OCS and CO," J. Mol. Spectrosc. **216**, 428–436 (2002).

09 March 2026 12:51:39

© Author(s) 2022

[18]J.-M. Colmont, L. Nguyen, F. Rohart, and G. Wlodarczak, "Lineshape analysis of the $J = 3 \leftarrow 2$ and $J = 5 \leftarrow 4$ rotational transitions of room temperature CO broadened by N_2, O_2, CO_2 and noble gases," J. Mol. Spectrosc. **246**, 86–97 (2007).
[19]D. Robert and J. Bonamy, "Short range force effects in semiclassical molecular line broadening calculations," J. Phys. **40**, 923–943 (1979).
[20]H. Jóźwiak, F. Thibault, H. Cybulski, and P. Wcisło, "*Ab initio* investigation of the CO–N_2 quantum scattering: The collisional perturbation of the pure rotational R(0) line in CO," J. Chem. Phys. **154**, 054314 (2021).
[21]I. E. Gordon, L. S. Rothman, R. J. Hargreaves, R. Hashemi, E. V. Karlovets, F. M. Skinner, E. K. Conway, C. Hill, R. V. Kochanov, Y. Tan, P. Wcisło, A. A. Finenko, K. Nelson, P. F. Bernath, M. Birk, V. Boudon, A. Campargue, K. V. Chance, A. Coustenis, B. J. Drouin, J. M. Flaud, R. R. Gamache, J. T. Hodges, D. Jacquemart, E. J. Mlawer, A. V. Nikitin, V. I. Perevalov, M. Rotger, J. Tennyson, G. C. Toon, H. Tran, V. G. Tyuterev, E. M. Adkins, A. Baker, A. Barbe, E. Canè, A. G. Császár, A. Dudaryonok, O. Egorov, A. J. Fleisher, H. Fleurbaey, A. Foltynowicz, T. Furtenbacher, J. J. Harrison, J. M. Hartmann, V. M. Horneman, X. Huang, T. Karman, J. Karns, S. Kassi, I. Kleiner, V. Kofman, F. Kwabia-Tchana, N. N. Lavrentieva, T. J. Lee, D. A. Long, A. A. Lukashevskaya, O. M. Lyulin, V. Y. Makhnev, W. Matt, S. T. Massie, M. Melosso, S. N. Mikhailenko, D. Mondelain, H. S. P. Müller, O. V. Naumenko, A. Perrin, O. L. Polyansky, E. Raddaoui, P. L. Raston, Z. D. Reed, M. Rey, C. Richard, R. Tóbiás, I. Sadiek, D. W. Schwenke, E. Starikova, K. Sung, F. Tamassia, S. A. Tashkun, J. Vander Auwera, I. A. Vasilenko, A. A. Vigasin, G. L. Villanueva, B. Vispoel, G. Wagner, A. Yachmenev, and S. N. Yurchenko, "The HITRAN2020 molecular spectroscopic database," J. Quant. Spectrosc. Radiat. Transfer **277**, 107949 (2022).
[22]G. Knizia, T. B. Adler, and H.-J. Werner, "Simplified CCSD(T)-F12 methods: Theory and benchmarks," J. Chem. Phys. **130**, 054104 (2009).
[23]K. A. Peterson, T. B. Adler, and H.-J. Werner, "Systematically convergent basis sets for explicitly correlated wavefunctions: The atoms H, He, B–Ne, and Al–Ar," J. Chem. Phys. **128**, 084102 (2008).
[24]D. Feller, K. A. Peterson, and T. D. Crawford, "Sources of error in electronic structure calculations on small chemical systems," J. Chem. Phys. **124**, 054107 (2006).
[25]R. Dawes and S. A. Ndengué, "Single- and multireference electronic structure calculations for constructing potential energy surfaces," Int. Rev. Phys. Chem. **35**, 441–478 (2016).
[26]H.-J. Werner, P. J. Knowles, G. Knizia, F. R. Manby, and M. Schütz, "Molpro: A general-purpose quantum chemistry program package," Wiley Interdiscip. Rev.: Comput. Mol. Sci. **2**, 242–253 (2012).
[27]E. Castro-Juárez, X.-G. Wang, T. Carrington, Jr., E. Quintas-Sánchez, and R. Dawes, "Computational study of the ro-vibrational spectrum of CO–CO_2," J. Chem. Phys. **151**, 084307 (2019).
[28]B. Desrousseaux, E. Quintas-Sánchez, R. Dawes, and F. Lique, "Collisional excitation of CF^+ by H_2: Potential energy surface and rotational cross sections," J. Phys. Chem. A **123**, 9637–9643 (2019).
[29]C. T. Bop, F. A. Batista-Romero, A. Faure, E. Quintas-Sánchez, R. Dawes, and F. Lique, "Isomerism effects in the collisional excitation of cyanoacetylene by molecular hydrogen," ACS Earth Space Chem. **3**, 1151–1157 (2019).
[30]E. Quintas-Sánchez, R. Dawes, X.-G. Wang, and T. Carrington, "Computational study of the rovibrational spectrum of CO_2–N_2," Phys. Chem. Chem. Phys. **22**, 22674–22683 (2020).
[31]B. Desrousseaux, E. Quintas-Sánchez, R. Dawes, S. Marinakis, and F. Lique, "Collisional excitation of interstellar PN by H_2: New interaction potential and scattering calculations," J. Chem. Phys. **154**, 034304 (2021).
[32]M. Gancewski, H. Jóźwiak, E. Quintas-Sánchez, R. Dawes, F. Thibault, and P. Wcisło, "Fully quantum calculations of O_2–N_2 scattering using a new potential energy surface: Collisional perturbations of the oxygen 118 GHz fine structure line," J. Chem. Phys. **155**, 124307 (2021).
[33]C. Balança, E. Quintas-Sánchez, R. Dawes, F. Dumouchel, F. Lique, and N. Feautrier, "Inelastic rate coefficients for collisions of C_4H^- with H_2," Mon. Not. R. Astron. Soc. **508**, 1148–1155 (2021).
[34]E. Quintas-Sánchez, R. Dawes, and O. Denis-Alpizar, "Theoretical study of the HCS^+–H_2 van der Waals complex: Potential energy surface, rovibrational bound states, and rotationally inelastic collisional cross sections," Mol. Phys. **119**, e1980234 (2021).
[35]E. Quintas-Sánchez and R. Dawes, "AUTOSURF: A freely available program to construct potential energy surfaces," J. Chem. Inf. Model. **59**, 262–271 (2019).
[36]R. Dawes and E. Quintas-Sánchez, "The construction of ab initio-based potential energy surfaces," in *Reviews in Computational Chemistry* (John Wiley & Sons, 2019), Vol. 31, Chap. 5, pp. 199–264.
[37]M. Majumder, S. A. Ndengue, and R. Dawes, "Automated construction of potential energy surfaces," Mol. Phys. **114**, 1–18 (2016).
[38]R. Dawes, X.-G. Wang, A. W. Jasper, and T. Carrington, Jr., "Nitrous oxide dimer: A new potential energy surface and rovibrational spectrum of the nonpolar isomer," J. Chem. Phys. **133**, 134304 (2010).
[39]I. M. Sobol, "Uniformly distributed sequences with an additional uniform property," USSR Comput. Math. Math. Phys. **16**, 236–242 (1976).
[40]S. Green, "Rotational excitation in H_2–H_2 collisions: Close-coupling calculations," J. Chem. Phys. **62**, 2271–2277 (1975).
[41]S. Green, "Raman linewidths and rotationally inelastic collision rates in nitrogen," J. Chem. Phys. **98**, 257–268 (1993).
[42]G. Gioumousis and C. F. Curtiss, "Molecular collisions. II. Diatomic molecules," J. Math. Phys. **2**, 96–104 (1961).
[43]H. Klar, "Theory of scattering between two rigid rotors," Z. Phys. A: Hadrons Nucl. **228**, 59–69 (1969).
[44]L. Monchick and L. W. Hunter, "Diatomic–diatomic molecular collision integrals for pressure broadening and Dicke narrowing: A generalization of Hess's theory," J. Chem. Phys. **85**, 713–718 (1986).
[45]J. Schäfer and L. Monchick, "Line broadening of HD immersed in He and H_2 gas," Astron. Astrophys. **265**, 859–868 (1992), https://ui.adsabs.harvard.edu/abs/1992A%26A...265..859S/abstract.
[46]A. Yutsis, I. Levinson, and V. Vanagas, *The Mathematical Apparatus of the Theory of Angular Momentum* (Israel Program for Scientific Translations Ltd., Jerusalem, 1962).
[47]H. Jóźwiak, M. Gancewski, A. Grabowski, A. Olejnik, K. Stankiewicz, A. Zadrożny, and P. Wcisło, BIGOS computer code.
[48]B. R. Johnson, "The renormalized Numerov method applied to calculating bound states of the coupled-channel Schroedinger equation," J. Chem. Phys. **69**, 4678–4688 (1978).
[49]J. M. Brown, J. M. Brown, and A. Carrington, *Rotational Spectroscopy of Diatomic Molecules* (Cambridge University Press, 2003).
[50]L. Gomez, S. V. Ivanov, O. G. Buzykin, and F. Thibault, "Comparison of quantum, semiclassical and classical methods in hydrogen broadening of nitrogen lines," J. Quant. Spectrosc. Radiat. Transfer **112**, 1942–1949 (2011).
[51]F. Thibault, R. Z. Martínez, D. Bermejo, and L. Gómez, "Collisional line widths of autoperturbed N_2: Measurements and quantum calculations," J. Quant. Spectrosc. Radiat. Transfer **112**, 2542–2551 (2011).
[52]P. Wcisło, F. Thibault, M. Zaborowski, S. Wójtewicz, A. Cygan, G. Kowzan, P. Masłowski, J. Komasa, M. Puchalski, K. Pachucki, R. Ciuryło, and D. Lisak, "Accurate deuterium spectroscopy for fundamental studies," J. Quant. Spectrosc. Radiat. Transfer **213**, 41–51 (2018).
[53]R. Hashemi, I. E. Gordon, E. M. Adkins, J. T. Hodges, D. A. Long, M. Birk, J. Loos, C. D. Boone, A. J. Fleisher, A. Predoi-Cross, and L. S. Rothman, "Improvement of the spectroscopic parameters of the air- and self-broadened N_2O and CO lines for the HITRAN2020 database applications," J. Quant. Spectrosc. Radiat. Transfer **271**, 107735 (2021).
[54]V. M. Devi, D. C. Benner, K. Sung, T. J. Crawford, G. Li, R. R. Gamache, M. A. H. Smith, I. E. Gordon, and A. W. Mantz, "Positions, intensities and line shape parameters for the $1 \leftarrow 0$ bands of CO isotopologues," J. Quant. Spectrosc. Radiat. Transfer **218**, 203–230 (2018).
[55]L. Régalia-Jarlot, X. Thomas, P. Von der Heyden, and A. Barbe, "Pressure-broadened line widths and pressure-induced line shifts coefficients of the (1-0) and (2-0) bands of $^{12}C^{16}O$," J. Quant. Spectrosc. Radiat. Transfer **91**, 121–131 (2005).
[56]P. Varanasi, "Measurement of line widths of CO of planetary interest at low temperatures," J. Quant. Spectrosc. Radiat. Transfer **15**, 191–196 (1975).
[57]K. Sung and P. Varanasi, "Intensities, collision-broadened half-widths, and collision-induced line shifts in the second overtone band of $^{12}C^{16}O$," J. Quant. Spectrosc. Radiat. Transfer **83**, 445–458 (2004).

09 March 2026 12:51:39

© Author(s) 2022

[58]P. Wcisło, F. Thibault, N. Stolarczyk, H. Jóźwiak, M. Słowiński, M. Gancewski, K. Stankiewicz, M. Konefał, S. Kassi, A. Campargue *et al.*, "The first comprehensive dataset of beyond-Voigt line-shape parameters from *ab initio* quantum scattering calculations for the HITRAN database: He-perturbed H_2 case study," J. Quant. Spectrosc. Radiat. Transfer **260**, 107477 (2021).

[59]K. Stankiewicz, N. Stolarczyk, H. Jóźwiak, F. Thibault, and P. Wcisło, "Accurate calculations of beyond-Voigt line-shape parameters from first principles for the He-perturbed HD rovibrational lines: A comprehensive dataset in the HITRAN DPL format," J. Quant. Spectrosc. Radiat. Transfer **276**, 107911 (2021).

09 March 2026 12:51:39

© Author(s) 2022